Proxies and Measurement Techniques for Mineral Dust in Antarctic Ice Cores

URS RUTH,*,[†] CARLO BARBANTE,[‡]
MATTHIAS BIGLER,[§,||]
BARBARA DELMONTE,[⊥]
HUBERTUS FISCHER,[†]
PAOLO GABRIELLI,[‡,#] VANIA GASPARI,[‡]
PATRIK KAUFMANN,[§]
FABRICE LAMBERT,[§] VALTER MAGGI,[⊥]
FEDERICA MARINO,[⊥,▽]
JEAN-ROBERT PETIT,[○]
ROBERTO UDISTI,[▽]
DIETMAR WAGENBACH,[◆]
ANNA WEGNER,[†] AND ERIC W. WOLFF[¶]

Alfred-Wegener-Institute for Polar and Marine Research, Bremerhaven, Germany, Department of Environmental Sciences, University of Venice, Venice, Italy, Climate and Environmental Physics, Physics Institute, University of Bern, Bern, Switzerland, Centre for Ice and Climate, Niels Bohr Institute, University of Copenhagen, Denmark, Department of Environmental Sciences, University of Milano Biccoca, Italy, School of Earth Sciences and Byrd Polar Research Center, Ohio State University, Columbus, Ohio, Department of Chemistry, University of Florence, Florence, Italy, Laboratoire de Glaciologie et Géophysique de l'Environnement, CNRS, Grenoble, France, Institut für Umweltphysik, University of Heidelberg, Heidelberg, Germany, and British Antarctic Survey, Cambridge, United Kingdom

To improve quantitative interpretation of ice core aeolian dust records, a systematic methodological comparison was made. This involved methods for water-insoluble particle counting (Coulter counter and laser-sensing particle detector), soluble ion analysis (ion chromatography and continuous flow analysis), elemental analysis (inductively coupled plasma mass spectroscopy at pH 1 and after full acid digestion), and water-insoluble elemental analysis (proton induced X-ray emission). Antarctic ice core samples covering the last deglaciation from the EPICA Dome C (EDC) and the EPICA Dronning Maud Land (EDML) cores were used. All methods correlate very well among each other, but the ratios of glacial age to Holocene concentrations, which are typically a factor ∼100, differ between the methods by up to a factor of 2 with insoluble particles showing the largest variability. The recovery of ICP-

* Corresponding author e-mail: Urs.Ruth@awi.de. Also at: Climate Analysis and Consulting, Germany.
[†] Alfred-Wegener-Institute for Polar and Marine Research.
[‡] University of Venice.
[§] University of Bern.
[||] University of Copenhagen.
[⊥] University of Milano Biccoca.
[#] Ohio State University.
[▽] University of Florence.
[○] CNRS.
[◆] University of Heidelberg.
[¶] British Antarctic Survey.

MS measurements depends on the digestion method and is different for different elements and during different climatic periods. EDC and EDML samples have similar dust composition, which suggests a common dust source or a common mixture of sources for the two sites. The analyzed samples further reveal a change of dust composition during the last deglaciation.

1. Introduction

Mineral dust aerosol is an important part of the climate system (*1–3*). Apart from sea salt it is the most abundant primary aerosol and influences the radiative energy budget of the atmosphere (*4*). Aeolian mineral dust can enhance primary marine bioproductivity (*5*) and can be important for pedogenesis in remote land areas (*6*). To understand the climate changes of the past it is therefore necessary to have an accurate quantitative reconstruction of the past atmospheric dust load and aeolian dust fluxes. Projects dedicated to this, such as DIRTMAP (*7*), rely on modeling studies and on dust accumulation data from environmental archives. Although most ice cores come from polar regions—which invokes complex transport processes from the midlatitude sources to high-latitude sites—they have a central role as dust archives because the dust is stored in the simple matrix of ultrapure water and because they offer excellent time control and temporal resolution.

The most common proxies for dust in ice cores are insoluble particle concentration, e.g. refs *8–14*, and Ca^{2+} ion concentration, e.g. refs *15–19*. These have been complemented over recent years by a large suite of other proxies with multiple measurement techniques for the soluble and insoluble fractions of the mineral dust aerosol. However, the term "dust" is often used without exactly specifying the proxy considered, and it is largely unknown how the different proxies relate quantitatively to each other, particularly under changing climatic conditions.

The objective of this paper is to present a systematic comparison of different proxies and measurement techniques for mineral dust in ice cores. All techniques investigated use melted samples; thus techniques based on light scattering on solid ice (*20, 21*) are omitted. The use of certified dust samples proved inappropriate because their size distribution, shape, optical properties, mineralogy, and elemental composition differ significantly from aeolian dust accumulated in polar ice cores. Instead, real ice core samples were used from the two deep drilling sites of the European Project for Ice Coring in Antarctica (EPICA): EPICA Dome C (EDC) (*22*) and EPICA Dronning Maud Land (EDML) (*23*). Each set of some 20 samples spans the last glacial termination (see Supporting Information (SI) Figure S1), which took place approximately 10−20 ka BP (thousand years before present). Thus, the samples cover the full range from low dust concentrations in the Holocene to high dust concentrations during the Last Glacial Maximum (LGM) and can also capture possible changes of dust composition over this important climatic transition. Methodological results from this study are expected to apply also to other ice cores from Antarctica or Greenland.

2. Materials and Methods

Ice samples were decontaminated by three repeated washings in ultrapure water (Millipore). The initial weight of each sample was about 200 g, and the mass loss during decontamination was ∼50%. The decontaminated samples were melted at room temperature in prewashed LDPE bottles.

TABLE 1. Parameter Overview: List of Species and Measurement Methods of Mineral Dust Discussed in This Paper (Also Given Are the Respective Limits of Detection (LOD, Including Procedural Blanks) for Typical Applications)

acronym	species	method	LOD [μg/kg]
CC-mass	total water-insoluble particle mass (from particle volume)	Coulter counter	2
LPD-mass	total water-insoluble particle mass (from particle diameter)	laser-sensing particle detector	1
IC-Ca	soluble Ca^{2+}	ion chromatography	2
CFA-Ca	soluble Ca^{2+}	continuous flow analysis	0.1
nss-CFA-Ca*	soluble nonsea-salt Ca^{2+}	calculated [$(Na/Ca)_{sol,dust} = 0.91$]	
ICPMS-digest-Al	total Al (full acid digestion)	ICP-MS	0.5
ICPMS-digest-Fe	total Fe (full acid digestion)	ICP-MS	0.2
ICPMS- HNO_3−Al	leachable Al (HNO_3-digestion at pH 1)	ICP-MS	0.1
ICPMS- HNO_3−Fe	leachable Fe (HNO_3-digestion at pH 1)	ICP-MS	0.03
ICPMS- HNO_3−V	leachable V (HNO_3-digestion at pH 1)	ICP-MS	0.001
PIXE-Al	water-insoluble, particulate dust Al	PIXE	0.8
PIXE-Ca	water-insoluble, particulate dust Ca	PIXE	0.2
PIXE-Fe	water-insoluble, particulate dust Fe	PIXE	0.1
PIXE-Si	water-insoluble, particulate dust Si	PIXE	0.7

Once melted, the samples were gently agitated for homogenization and then partitioned into individual vials (polystyrene Coulter-Counter accuvettes, precleaned using ultrapure water) for the different analyses. Repeated checks show that the dust concentration difference between the first and the last aliquots is typically around the level of measurement-reproducibility, i.e., the aliquots provided for the different analyses should be comparable. Exceptionally larger differences (up to 50%) were observed, probably due to contamination of selected aliquots. The washing and partitioning was performed in a class 100 laminar flow bench situated inside a class 1000 clean laboratory. The samples dedicated to insoluble particle analyses were analyzed promptly after melting; all other samples were refrozen within several hours, shipped frozen to the respective laboratories, and kept at −20 °C. The samples were then prepared for the respective analyses (Table 1) as described hereafter.

2.1. Insoluble Particles: Coulter Counter (CC). For Coulter Counter (CC) analysis an electrolyte (NaCl) was added to the sample, which was then pumped through a small orifice. The electrical conductance was measured across the orifice. Particles flowing through the orifice reduce the conductance, from which the total volume of each microparticle was directly estimated. A Multisizer IIe (Beckmann-Coulter) set up in the clean room of LGGE was used with a 50 μm orifice, allowing measurement of particles with diameters between 0.7 and 20 μm (256 size channels). Procedures are described elsewhere (11, 24). Size calibration was achieved via a certified standard of spherical latex particles (Beckman-Coulter). Each sample was measured three times with 0.5 mL sample volume per measurement. For calculation of the microparticle mass an average mineral density of 2.5 g/cm^3 was assumed.

2.2. Insoluble Particles: Laser-Sensing Particle Detector (LPD). A field-portable laser-based detection system LDS 23/25 (Klotz) was used, which was developed in cooperation with the University of Heidelberg. The liquid sample was pumped through a detection cell, where the attenuation of transmitted light (680 nm) was measured for each particle (32 channels). Conversion of this signal to particle size is difficult because complex scattering processes occur. Size assignment was obtained by a posteriori alignment of the LPD size spectra to the CC size spectra (Ruth et al., in preparation). Using this procedure, a lower particle detection limit of 1.04 μm diameter was found. The particle mass below this limit was estimated from a log-normal fit to the data (25) assuming a single-mode distribution. Each sample was measured three times with 2 mL per measurement. A mean density of 2.5 g/cm^3 was used to convert particle volume to mass.

2.3. Soluble Calcium: Ion Chromatography (IC). Ion chromatography (IC) is a commercially available method to quantify soluble major ion concentrations and is well-established for measurement of Ca^{2+} in ice cores (18, 19, 26). A sample loop of 1 mL was used with Dionex CG12A and CS12A guard and separation columns in an isocratic run using methanesulfonate eluent (20 mM); low background conductivity and noise was accomplished using autosuppression (Dionex CSRS Ultra II). Standardization was achieved by use of cation solutions of certified concentrations. The error for Ca^{2+} concentration is strongly dependent on the blank contribution and variability (typically 1 ± 1 μg/kg). With this blank variability, the reproducibility is better than 10% for concentrations larger than 20 μg/kg (i.e., samples from LGM) but increases to ±100% for concentrations of 1 μg/kg (i.e., samples from the Holocene). Each sample was measured once with 3 mL per sample.

2.4. Soluble Calcium: Continuous Flow Analysis (CFA) Fluorimetry. CFA is an established technique for continuous measurement of selected ion concentrations at high spatial resolution in ice cores (27). The analytical method (28) to quantify soluble Ca^{2+} ion concentrations was adapted at the University of Bern for CFA use (29). In a continuous flow reactor Ca^{2+} was converted at pH 7 to a fluorescent complex. The concentration was deduced from the fluorescence intensity, which was measured by a custom-made spectrometer at 495 nm wavelength. Standardization was achieved by use of certified Ca^{2+}-solutions. The method has a detection limit of 0.1 μg/kg. Typically, the sample water is obtained continuously from an ice-core melting device, but for this study discrete samples were injected into the system. Each sample was measured once with ∼5 mL per sample.

2.5. Elemental Concentrations: Inductively Coupled Plasma Mass Spectrometry. The samples for inductively coupled plasma mass spectrometry (ICP-MS) were subdivided at the University of Venice to compare two different sample preparation methods. For determination of the "acid-leachable" fractions the samples were melted and acidified to pH 1 with ultrapure nitric acid (Romil) 24 h prior to the analysis. For determination of the total content the samples underwent an acid digestion for complete dissolution: to 1 mL of melted sample were added about 0.3 mL of HNO_3 and 0.3 mL of HF (both ultrapure, Romil) with subsequent microwave irradiation in a PTFE pressure bomb. Procedural were prepared to check for contamination; and blank values were subtracted from the measured sample concentrations. Sector field ICP-MS (Element2, Thermo Finnigan) (30, 31) analyses were performed for aluminum (^{27}Al), vanadium (^{51}V), iron (^{56}Fe), and other trace elements at medium resolution ($m/\Delta m = 4000$) allowing for separation of major interferences

for Fe such as $^{40}Ar^{16}O$. Standardization was achieved using HNO_3-acidified and digested dilutions, respectively, of a multielement standard (Merck) (*32*).

2.6. Insoluble Element Concentrations: Proton Induced X-ray Emission (PIXE). PIXE is an X-ray spectrometry technique based on primary ionization of the inner electron-shells of a target atom by an impinging proton beam. The production of characteristic X-rays allows for highly sensitive bulk dust analysis of elements with atomic numbers ranging from 11 (Na) to 92 (U) (*33*). For analysis of Antarctic ice dust at very low concentrations, PIXE is able to measure Na, Mg, Al, Si, K, Ca, Ti, Mn, and Fe with analytical detection limits <1 μg/kg. PIXE targets were prepared directly by filtering each melted sample through a polycarbonate membrane (Nuclepore, pore size 0.45 μm) without pretreatment such as acidification or precipitation (*34*). Sample preparation was performed inside a class 100 laminar-flow bench inside a clean laboratory at the University of Milano-Bicocca. Procedural blanks were prepared by filtration of ultrapure water following identical procedures. The PIXE analyses were carried out at the 2 MeV AN2000 accelerator at the National Laboratories of Legnaro (Padova) (*34–36*). One target was prepared from each sample with sample volumes from 7 to 50 mL.

3. Results: Methodological Comparison

In total, more than 50 different species related to mineral dust were measured, but only the most relevant ones are discussed here. In this section, an overview of the results is given first followed by selected comparisons. Most plots shown are logarithmic scatter plots. Linear regression lines calculated from the logarithms of the data are also shown: EDML and EDC data combined (black, continuous line), EDC data only (red, dashed line), and EDML data only (blue, dotted line). Additionally, in the scatter plots some statistical measures are given; they are evaluated for the combined sets of EDML and EDC data: R_{log} is the correlation coefficient R calculated from the logarithms of the data. c_{log} is the slope of the linear regression line calculated from the logarithms of the data; a slope $\neq 1$ means that the y/x-ratio changes with concentration; the values given correspond to the slopes of the black regression lines. *median-ratio* is the median of all ratios y_i/x_i, where y_i is the species of the y-axis and x_i is the species of the x-axis for every data point i; *median-ratio* gives the typical ratio of the y-parameter to the x-parameter. *rel-gain* is the relative concentration increase of the y-parameter for an increase of the x-parameter by a factor f = 100; this is a measure of the sensitivity of the y-parameter to changes of the x-parameter in linear space. *rel-gain* = 0.5 means that for a 100-fold increase of the x-parameter the y-parameter increases by 50. Note that *rel-gain* = $f^{(c_{log}-1)}$, i.e. *rel-gain* does not transform linearly for factors $f \neq 100$.

3.1. Overview of Most Important Proxies and Methods. Figure 1 shows an overview of scatter plots for different species. See SI Figure S2 for a more comprehensive presentation. For purposes of comparability, they are all plotted against a common reference, for which insoluble particle concentrations (from CC) are chosen. The dust concentration in the EDML samples is typically 2−3 times that of EDC samples. Insoluble particles exhibit the largest concentration variance of all species shown; the ratio between highest glacial and lowest Holocene particle concentration is about 200 (119 for EDC and 337 for EDML for the particular sets of samples from this study). All chemical species exhibit a good correlation with insoluble particles, typically $R_{log} > 0.9$. However, c_{log} is >0.8, and *rel-gain* > 0.5 for most species, which means that the y/x-ratio is up to a factor of 2 lower at high than at low concentrations. This indicates considerable changes in dust composition or detection between the
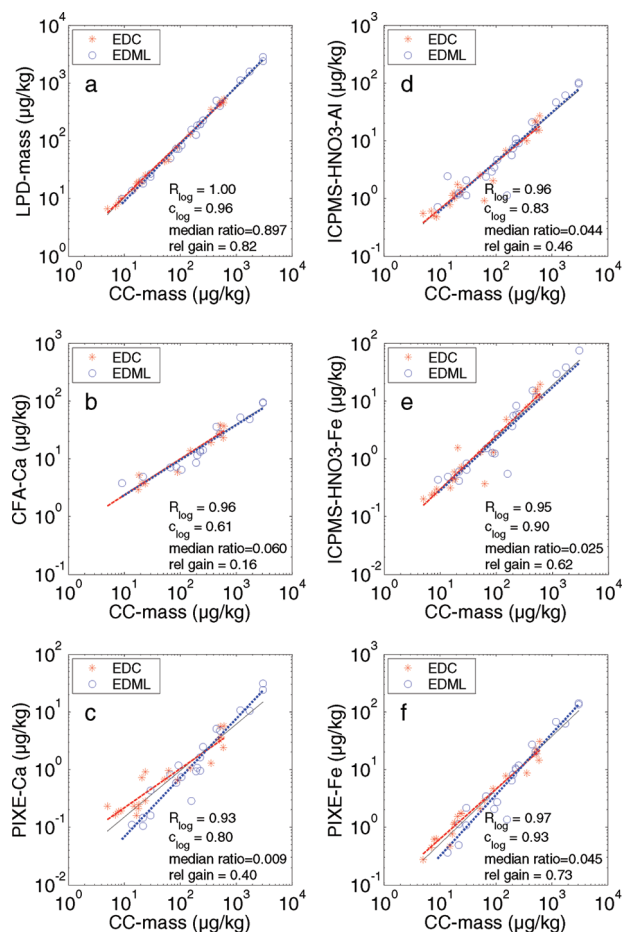

FIGURE 1. Scatter plots of different parameters all plotted vs insoluble particle mass (from Coulter counter) as a common reference for comparison. Note logarithmic scales. Shown also are linear regression lines calculated from the logarithms of the data: EDML and EDC data (black continuous line), EDC data only (red dashed line), and EDML data only (blue dotted line). Selected statistical measures are given in each plot for all (EDC and EDML) data: R_{log}, correlation coefficient (in loglog-space); c_{log}, slope of linear regression line (in loglog-space); *median ratio*, median of ratios (y_i/x_i) of concentrations; *rel-gain*,- relative gain of y-parameter for a concentration increase of factor 100 for the x-parameter. For details see text; for abbreviations of parameters see Table 1; see SI Figure S2 for a more comprehensive presentation.

climate regimes. Thus, a quantitative reconstruction of dust deposition fluxes will depend on the particular choice of the parameter.

3.2. Insoluble Particles. The comparison of LPD vs CC data of insoluble particle mass concentrations is shown in Figure 1a. While the CC is an established technique for measurement of discrete samples (*10, 11*), the LPD is a novel ice core method that is capable of CFA operation (*25*). The data have a very high correlation ($R_{log} = 1.00$); and the c_{log} of 0.96 is very close to 1. Good correspondence ($R_{log} = 1.00$ and $c_{log} = 0.92$) is found also between the respective number concentrations (data not shown). The very low scatter of the data suggests that the LPD is a reliable method to quantify variations of insoluble particle concentrations in ice cores; this is not a consequence of using CC data for the size calibration of the LPD because changes of mass concentration are caused primarily by changes of particle numbers and not of particle size. The *median-ratio* of 0.90 and the *rel-gain* of 0.82 show, however, that the LPD does not fully reproduce the large variance of the CC data; this may possibly result from coincidence losses (a particle passing while the detector
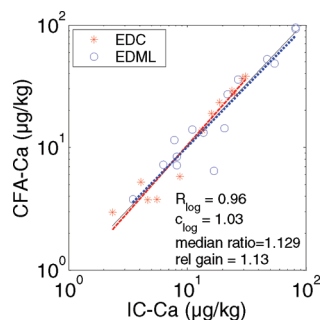
FIGURE 2. Scatter plot of CFA-Ca^{2+} vs IC-Ca^{2+}.

is still busy evaluating the previous particle), which are compensated for in the CC but not in the LPD. Altogether, the LPD vs CC plots show the smallest amount of scatter, which presumably is the consequence of the two methods both counting particles and also of the high precision of both methods.

3.3. Soluble Calcium. Unfortunately, there is evidence for possible analytical shortcomings regarding the determination of Ca^{2+} in this particular study. Part of the early Holocene samples from this study showed unrealistically high Ca^{2+} concentrations when compared to the exhaustive profiles available from EDC (*18*) and EDML (*19*) and were therefore excluded from the data set. This applied to IC as well as CFA data. In addition, the low *rel-gain* for Ca^{2+} reported here (see below) is not in agreement with previous data for EDC (*18, 22*) and EDML (*19, 23*), where similar factors were found for insoluble particles and Ca^{2+}. Thus, this section should be viewed with caution as there may be unidentified analytical problems for low concentrations.

Figures 1b, S2b, and S2e show the total Ca^{2+} and the nssCa^{2+} (nonsea-salt, see Section 4.2) ion concentrations vs insoluble particles. The correlation is high ($R = 0.96$ for each); but the c_{log} of only 0.61 and 0.69 and the *rel-gain* of only 0.16 and 0.24, respectively, are unexpectedly low.

A methodological comparison for IC measurements and CFA measurements is shown in Figure 2. The methods show a good correspondence with $R_{log} = 0.96$, *median-ratio* = 1.13, $c_{log} = 1.03$, and *rel-gain* = 1.13. This confirms good results from earlier comparisons (*26*), possibly with a higher scatter for IC measurements due to a higher blank contribution.

3.4. ICP-MS: Acidification to pH 1 and Full Digestion. Comparing elemental concentrations measured by ICP-MS to insoluble particle concentrations (Figures 1 and S2), R_{log} are all very high (0.93−0.96). c_{log} ranges from 0.83 (Al-HNO$_3$) to 0.93 (V-HNO$_3$). Vanadium (V) shows the best *rel-gain* (0.72). This confirms that V is a good proxy of Antarctic dust as there are no other sources even during interglacial periods (*37*).

The method of sample preparation has a large influence on the results obtained from ICP-MS measurements. A full acid digestion is expected to yield total element concentrations; but this method poses a significantly larger risk of contamination than an acidification to pH 1 using ultrapure HNO$_3$. In Figure 3 results obtained with these two sample preparation methods are compared for the major crustal elements Fe and Al. The correlation is generally good; but there is considerably larger variability for the early Holocene samples. For the species shown this higher variability is not a problem of detection limit or blank, nor a statistical consequence of smaller concentrations; instead, it points to enhanced compositional variations possibly related to variations of mineral identity of the dust during the Holocene.

By assuming 100% recovery for full acid digestion, the recovery of the pH 1 acidification can be quantified. This is found to vary between climatic periods. For the early Holocene samples the recovery is ∼30% (Fe), and 45% (Al)
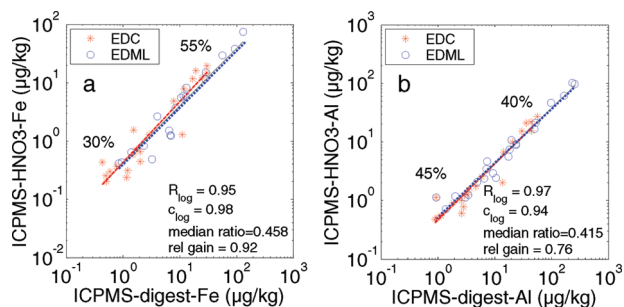

FIGURE 3. Scatter plot of ICP-MS element concentrations of Fe (a) and Al (b) for two different sample preparation techniques: acidification to pH 1 (y-axis) vs full acid digestion (x-axis). Typical recoveries of HNO$_3$-digestion (pH 1) are indicated for Holocene and LGM samples (see text for details).
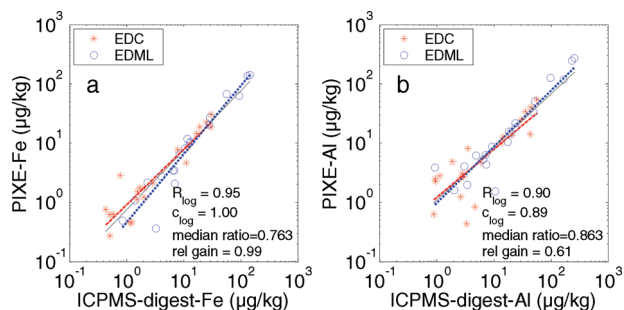

FIGURE 4. Scatter plot of PIXE vs ICP-MS (full digestion) for Fe (a) and Al (b).

with large scatter; for the late glacial samples the recovery is ∼55% (Fe) and 40% (Al). This confirms earlier findings of a 30−65% recovery for Fe (*32*). The recovery at pH 1 is least variable for Al, which should therefore be the preferred reference element when assessing variations of terrestrial enrichment factors from pH 1 digested samples. Unfortunately, blank problems in the full acid digested samples prevent a check on the robustness of the recovery rate for V at pH 1.

3.5. PIXE. Comparing elemental concentrations measured by PIXE to insoluble particle concentrations (Figures 1 and S2) R_{log} ranges from 0.92 (Al) to 0.97 (Si, Fe) with c_{log} from 0.8 (Ca) to 0.97 (Si). For Ca (Figure 1c) low concentration data give a different ratio between the two methods for EDC and EDML; however, concentrations are close to the detection limit.

PIXE measures the elemental composition of water-insoluble dust after filtration. By assuming 100% filtration efficiency for PIXE and 100% recovery for ICP-MS measurements (full acid digestion), the elements Fe and Al can be attributed to a water-insoluble fraction and a soluble residual. In Figure 4 results obtained with the two methods are compared.

For Fe a very good log-correlation is found ($R_{log} = 0.95$) with $c_{log} = 1.0$. The *median-ratio* is 0.76, suggesting that ∼25% of the Fe is water-soluble. This ratio does not change between glacial times and early Holocene. The upper limit for the fraction of bioavailable iron, which still depends on the oxidation state, would thus be ∼25%, which is larger by a factor 5−10 than the values typically used in models for simulating the effect of iron-fertilization in the Southern Ocean (*38–40*).

For Al the insoluble fraction amounts to ∼100%. However, early Holocene samples show a large scatter (especially for EDC samples) with PIXE concentrations exceeding the ICP-MS concentrations. This may be caused by analytical uncertainties with the ICP-MS full acid digestion method in this case.

A comparison between CFA-Ca (Figure 1b, mean concentration ~10 μg/kg) and PIXE-Ca (Figure 1c, mean concentration ~1 μg/kg) suggests that ~90% Ca is present in soluble form while only 10% is water-insoluble; this confirms and quantifies earlier findings (*3, 16, 35*).

4. Discussion of Dust Composition

The most noticeable observation from Figures 1–4 is that no obvious systematic differences occur between EDC and EDML samples. In all scatter plots shown, the samples from EDC and EDML overlap strongly and do not fall into separate groups. An exception is PIXE-Ca data during early Holocene, however, values are close to the detection limit and thus questionable. This suggests that the dust composition is geochemically very similar at the two sites and that they likely received dust from a common dust source or the same mixture of sources as has been suggested also for other locations (*41*).

The mean composition of the insoluble dust can be characterized by referring elemental concentrations determined by PIXE to the total particle mass from CC. This yields mean ratios of approximately 0.26 (Si), 0.08 (Al), and 0.05 (Fe), which deviate only slightly from the mean composition of upper continental crust of 0.30 (Si), 0.08 (Al), and 0.03 (Fe) (*42*). Detailed compositional investigations should be made using material from potential dust sources and focusing on fractionation during uptake, atmospheric transport, and dissolution.

Although the mean composition for Si, Al, Fe, and Ca as referenced to CC insoluble particle mass gives reasonable results similar to crustal averages, the *rel-gain* is always below 1. This could imply that either the dust is depleted in these elements at high concentrations or enriched at low concentrations, possibly resulting from fractionation during transport. Alternatively, there could be analytical issues, and further work is needed to clarify this issue.

4.1. Terrestrial vs Marine Contributions to Ca^{2+} and Na^+. Ca^{2+} and Na^+ contain soluble terrestrial contributions from mineral dust and marine contributions from sea salt. To evaluate these contributions separately the respective mass ratios $(Na/Ca)_{sol,dust}$ of soluble Na^+ and Ca^{2+} from mineral dust and $(Na/Ca)_{ss}$ from sea salt aerosol must be known. $(Na/Ca)_{ss}$ ranges between 23 (brine rejected during sea ice formation (*43*)) and 26 (bulk seawater (*44*)). However, $(Na/Ca)_{sol,dust}$ is far more variable and less well-known.

The apportionment of Ca^{2+} into a "non sea salt" fraction (nssCa) and a "sea salt" fraction (ssCa) often considers $(Na/Ca)_{sol,dust} = 0.56$ (e.g., refs *3, 45*), which corresponds to the total (not only soluble) elemental composition of mean continental crust (*44*). Alternatively, total element ratios for upper continental crust could be used (Na/Ca = 0.87) (*42*); and from high-resolution ice core data $(Na/Ca)_{sol,dust} = 0.94 \pm 0.07$ is suggested (*46*). Here we take another complementary approach based on linking insoluble dust, Ca^{2+} and Na^+ concentrations. The following equations are considered: $[Ca^{2+}] = [Ca_{ss}] + [Ca_{sol,dust}] = \alpha^{-1} [Na_{ss}] + a [CC]$, where $\alpha = (Na/Ca)_{ss}$ is chosen to be 26 ($\alpha = 23$ gives the same results for b), $a = [Ca_{sol,dust}]/[CC]$, and [CC] is the insoluble particle mass concentration. Further, $[Na^+] = [Na_{ss}] + [Na_{sol,dust}] = [Na_{ss}] + ab [CC]$, where $b = (Na/Ca)_{sol,dust}$ is the parameter of interest. Parameter optimization yields $b = 0.91 \pm 0.2$ ($a = 0.085$) for all samples from this study [$b = 1.05$ ($a = 0.057$) for samples dated older than 16 ka BP to circumvent potential problems with Holocene Ca^{2+} data, and $b = 0.83$ ($a = 0.092$) for samples dated younger than 16 ka BP]. Thus, we suggest an average of $(Na/Ca)_{sol,dust} = 0.91 \pm 0.2$ by mass, which is in good agreement with ref (*46*).

4.2. Temporal Changes of Dust Composition. Compositional changes of the ice core dust over time can be
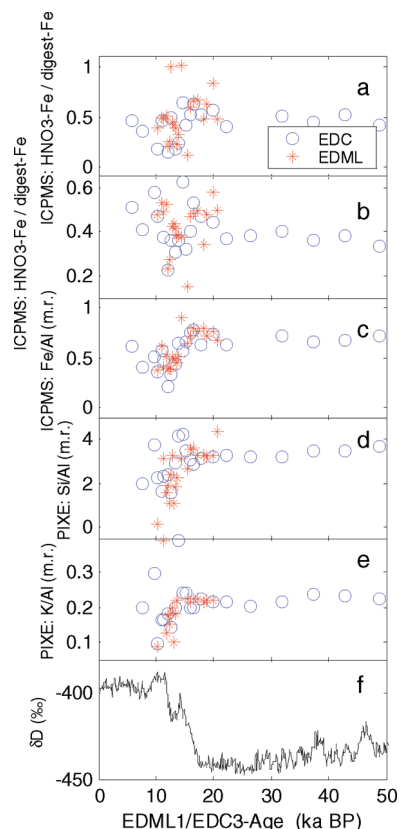

FIGURE 5. Time series of different ratios of element concentrations shown on the common *EDML1/EDC3* time scale (*47, 48*): ICP-MS concentrations of HNO_3-digestion (pH 1) normalized to full acid digestion of Fe (a) and Al (b); Fe/Al mass ratio of ICP-MS concentrations (HNO_3-digestion) (c); PIXE concentrations of Si (d) and K (e) both normalized to PIXE-Al concentrations (expressed as mass ratios, m.r.). A regime shift at ~16 ka BP is noticeable from changing point-to-point variability and value of some ratios. For orientation, the EDC deuterium isotopic deviation as a proxy for atmospheric temperature is shown (*22*).

identified by calculating ratios between different dust-related parameters on identical ice-core samples. Figure 5 shows time series of selected ratios on the common *EDML1/EDC3* time scale (*47, 48*): the recovery of ICP-MS measurements for sample preparation at pH 1 for Fe and Al, the Fe/Al ratio at pH 1, and the element ratios Si/Al and K/Al from PIXE. It is clearly noticeable that a regime-shift happens during the deglaciation. The sample-to-sample variability of the ratios is much higher for the early Holocene samples than for the late glacial samples. Also, the average recovery of acidified samples (pH 1) measured by ICP-MS changes during the deglaciation, albeit less prominently. Further, the insoluble elemental composition of the dust (PIXE) shifts to relatively more Al, less Si, and less K.

There have been other indications of a changing dust mineralogy during the last deglaciation: A similar shift to less K and more Ca in the Taylor Dome ice core (*49*), and a difference of Nd and Sr isotope ratios at EDC (*50*) and a change of Li solubility at EDC (*51*). This regime shift dates between ~16.5 and ~15.0 ka BP from our data. It suggests that either the characteristics of the dust source changed (e.g., soil development), or there was a change in the relative contributions of different sources (e.g., transport changes). The overlap of EDC and EDML samples indicates that even at times of higher variability there are no distinct sources and transport paths to the two ice core sites. Thus, the controlling factors for dust concentrations on the East

Antarctic plateau likely are the emission intensity in the dust sources as well as the ability of the dust to intrude the polar vortex. Once inside the polar vortex the dust transport to the two sites is either very homogeneous or effectively randomized.

Acknowledgments

Supporting Information Available

This material is available free of charge via the Internet at http://pubs.acs.org.

Literature Cited

(1) Prospero, J. M.; Charlson, R. J.; Mohnen, V.; Jaenicke, R.; Delany, A. C.; Moyers, J.; Zoller, W.; Rahn, K. The atmospheric aerosol system: an overview. *Rev. Geophys. Space Phys.* **1983**, *21* (7), 1607–1629.

(2) Rea, D. K. The paleoclimatic record provided by eolian deposition in the deep sea: the geologic history of wind. *Rev. Geophys.* **1994**, *32* (2), 159–195.

(3) Fischer, H.; Siggaard-Andersen, M. L.; Ruth, U.; Röthlisberger, R.; Wolff, E. Glacial/interglacial changes in mineral dust and sea-salt records in polar ice cores: Sources, transport, and deposition. *Rev. Geophys.* **2007**, *45*, . (RG1002), doi:10.1029/2005RG000192.

(4) Sokolik, I. N.; Winker, D. M.; Bergametti, G.; Gillette, D. A.; Carmichael, G.; Kaufman, Y. J.; Gomes, L.; Schuetz, L.; Penner, J. E. Introduction to special section: Outstanding problems in quantifying the radiative impacts of mineral dust. *J. Geophys. Res.* **2001**, *106* (D16), 18015–18027.

(5) Boyd, P. W.; Jickells, T.; Law, C. S.; Blain, S.; Boyle, E. A.; Buesseler, K. O.; Coale, K. H.; Cullen, J. J.; de Baar, H. J. W.; Follows, M.; Harvey, M.; Lancelot, C.; Levasseur, M.; Owens, N. P. J.; Pollard, R.; Rivkin, R. B.; Sarmiento, J.; Schoemann, V.; Smetacek, V.; Takeda, S.; Tsuda, A.; Turner, S.; Watson, A. J. Mesoscale Iron Enrichment Experiments 1993−2005: Synthesis and Future Directions. *Science* **2007**, *315*, 612–617; DOI: 10.1126/science.1131669.

(6) Wang, P.; Clemens, S. C.; Beaufort, L.; Branconnot, P.; Ganssen, G. M.; Jian, Z.; Kershaw, P.; Sarnthein, M. Evolution and variability of the Asian monsoon system: State of the art and outstanding issues. *Quat. Sci. Rev.* **2005**, *24*, 595–629.

(7) Kohfeld, K. E.; Harrison, S. P. DIRTMAP: the geological record of dust. *Earth-Sci. Rev.* **2001**, *54*, 81–114.

(8) Cragin, J. H.; Herron, M. M.; Jr.; Klouda, G. Interhemispheric comparison of changes in the composition of atmospheric precipitation during the late Cenozoic era. In *Polar Oceans*; Dunbar, M. J., Ed.; Arctic Institute of North America: Calgary, AB, Canada, 1977; pp 617−631.

(9) Hammer, C. U. In *Dust Studies on Greenland Ice Cores*, Isotopes and impurities in snow and ice-symposium, Proceedings of the Grenoble Symposium, 1977; pp 365−370.

(10) Petit, J.-R.; Briat, M.; Royer, A. Ice age aerosol content from East Antarctic ice core samples and past wind strength. *Nature* **1981**, *293*, 391–394.

(11) Steffensen, J. P. The size distribution of microparticles from selected segments of the Greenland Ice Core Project ice core representing different climatic periods. *J. Geophys. Res.* **1997**, *102* (C12), 26755–26763.

(12) Delmonte, B.; Basile-Doelsch, I.; Petit, J.-R.; Maggi, V.; Revel-Rolland, M.; Michard, A.; Jagoutz, E.; Grousset, F. E. Comparing the EPICA and Vostok dust records during the last 220,00 years: stratigraphical correlation and provenance in glacial periods. *Earh-Sci. Rev.* **2004**, *66*, 63–87.

(13) Ruth, U.; Bigler, M.; Röthlisberger, R.; Siggaard-Andersen, M.-L.; Kipfstuhl, S.; Goto-Azuma, K.; Hansson, M. E.; Johnsen, S. J.; Lu, H.; Steffensen, J. P. Ice core evidence for a very tight link between North Atlantic and east Asian glacial climate. *Geophys. Res. Lett.* **2007**, *34*, . (L03706), doi:10.1029/2006GL027876.

(14) Lambert, F.; Delmonte, B.; Petit, J.-R.; Bigler, M.; Kaufmann, P.; Hutterli, M. A.; Stocker, T.; Ruth, U.; Steffensen, J. P.; Maggi, V. Dust-climate couplings over the past 800,000 years from the EPICA Dome C ice core. *Nature* **2008**, *452*, 616–619.

(15) Legrand, M.; Delmas, R. Soluble impurities in four Antarctic ice cores over the last 30000 years. *Ann. Glaciol.* **1988**, *10*, 116–120.

(16) de Angelis, M.; Barkov, N. I.; Petrov, V. N. Sources of continental dust over Antarctica during the last glacial cycle. *J. Atmos. Chem.* **1992**, *14*, 233–244.

(17) Mayewski, P. A.; Meeker, L. D.; Whitlow, S.; Twickler, M. S.; Morrison, M. C.; Bloomfield, P.; Bond, G. C.; Alley, R. B.; Gow, A. J.; Grootes, P. M.; Meese, D. A.; Ram, M.; Taylor, K. C.; Wumkes, W. Changes in atmospheric circulation and ocean ice cover over the North Atlantic during the last 41,000 years. *Science* **1994**, *263*, 1747–1751.

(18) Wolff, E. W.; Fischer, H.; Fundel, F.; Ruth, U.; Twarloh, B.; Littot, G.; Mulvaney, R.; Röthlisberger, R.; de Angelis, M.; Boutron, C.; Hansson, M.; Jonsell, U.; Hutterli, M.; Bigler, M.; Lambert, F.; Kaufmann, P.; Stauffer, B.; Steffensen, J. P.; Siggaard-Andersen, M. L.; Udisti, R.; Becagli, S.; Castellano, E.; Severi, M.; Wagenbach, D.; Barbante, C.; Gabrielli, P.; Gaspari, V. Southern Ocean sea-ice extent, productivity and iron flux over the past eight glacial cycles. *Nature* **2006**, *440*, 491–496; doi:10.1038/nature04614.

(19) Fischer, H.; Fundel, F.; Ruth, U.; Twarloh, B.; Wegner, A.; Udisti, R.; Becagli, S.; Castellano, E.; Morganti, A.; Severi, M.; Wolff, E.; Littot, G.; Röthlisberger, R.; Mulvaney, R.; Hutterli, A.; Kaufmann, P.; Federer, U.; Lambert, F.; Bigler, M.; Hansson, M.; Jonsell, U.; de Angelis, M.; Gabrielli, P.; Boutron, C.; Siggaard-Andersen, M. L.; Steffensen, J. P.; Barbante, C.; Gaspari, V.; Gabrielli, P.; Wagenbach, D. Reconstruction of millenial changes in dust emission, transport and regional sea ice coverage using the deep EPICA ice cores from the Atlantic and Indian Ocean sectors of Antarctica. *Earth Planet. Sci. Lett.s* **2007**, *260*, 340–354.

(20) Bay, R. C.; Price, B. P.; Clow, G. D.; Gow, A. J. Climate logging with a new rapid optical technique at Siple Dome. *Geophys. Res. Lett.* **2001**, *28* (24), 4635–4638.

(21) Ram, M.; Koenig, G. Continuous dust concentration profile of pre-Holocene ice from the Greenland Ice Sheet Projct 2 ice core: dust stadials, interstadials, and the Eemian. *J. Geophys. Res.* **1997**, *102* (C12), 26641–26648.

(22) EPICA community members. Eight glacial cycles from an Antarctic ice core. *Nature* **2004**, *429*, 623–628.

(23) EPICA community members. One-to-one coupling of glacial climate variability in Greenland and Antarctica. *Nature* **2006**, *444*, 195–198.

(24) Delmonte, B.; Petit, J. R.; Maggi, V. Glacial to Holocene implications of the new 27,000-year dust record from the EPICA Dome C (East Antarctica) ice core. *Climate Dynamics* **2002**, *18* (8), 647–660.

(25) Ruth, U.; Wagenbach, D.; Steffensen, J. P.; Bigler, M. Continuous record of microparticle concentration and size distribution in the central Greenland NGRIP ice core during the last glacial period. *J. Geophys. Res.* **2003**, 108. (D3), doi:10.1029/2002JD002376.

(26) Littot, G.; Mulvaney, R.; Röthlisberger, R.; Udisti, R.; Wolff, E.; Castellano, E.; de Angelis, M.; Hansson, M. E.; Sommer, S.; Steffensen, J. P. Comparison of analytical methods used for measuring mahor ions in the EPICA Dome C (Antarctica) ice core. *Ann. Glaciol.* **2002**, *35*, 299–305.

(27) Röthlisberger, R.; Bigler, M.; Hutterli, A.; Sommer, S.; Stauffer, B.; Junghans, H. G.; Wagenbach, D. Technique for continuous high-resolution analysis of trace substances in firn and ice cores. *Environ. Sci. Technol.* **2000**, *34*, 338–342.

(28) Tsien, R. Y.; Pozzan, T.; Rink, T. J. Calcium homeostasis in intact lymphocytes: cyroplasmic free calcium monitored with a new, intracellularly trapped fluorecent indicator. *J. Cell Biol.* **1982**, *94*, 325–334.

(29) Sigg, A.; Fuhrer, K.; Anklin, M.; Staffelbach, T.; Zurmühle, D. A continuous analysis technique for trace species in ice cores. *Environ. Sci. Technol.* **1994**, *28*, 204–210.

(30) Barbante, C.; Cozzi, G.; Capodaglio, G.; van de Velde, K.; Ferrari, C.; Boutron, C.; Cescon, P. Trace element determination in alpine snow and ice by double focussing inductively coupled plasma spectrometry. *J. Anal. Atom. Spectrom.* **1999**, *14*, 1433.

(31) Planchon, F. A. M.; Boutron, C.; Barbante, C.; Wolff, E. W.; Cozzi, G.; Gaspari, V.; Ferrari, C.; Cescon, P. Ultrasensitive determination of heavy metals at the sub-picogram per gram level in ultraclean Antarctic snow samples by inductively coupled plasma sector field mass spectrometry. *Anal. Chim. Acta* **2001**, *450* (1), 193–205.

(32) Gaspari, V.; Barbante, C.; Cozzi, G.; Cescon, P.; Boutron, C.; Gabrielli, P.; Capodaglio, G.; Ferrari, C.; Petit, J. R.; Delmonte, B. Atmospheric iron fluxes over the last deglaciation: climatic implications. *Geophys. Res. Lett.* **2006**, *33*, L03704; doi:10.1029/2005GL024352.

(33) Johansson, S. A. E.; Campbell, J. L.; Malmqvist, K. L. *Particle Induced X-ray Emission (PIXE)*; John Wiley and Sons, Inc.: New York, 1995.

(34) Marino, F.; Maggi, V.; Delmonte, B.; Ghermandi, G.; Petit, J.-R. Elemental composition (Si, Fe, Ti) of atmospheric dust over the last 220 kyr from the EPICA ice core (Dome-C, Antactica). *Ann. Glaciol.* **2004**, *39*, 110–118.

(35) Ghermandi, G.; Cecchi, R.; Capotosto, M.; Marino, F. Elemental composition determined by PIXE analysis of the insoluble aerosol particles in EPICA-Dome C ice core samples representing the last 27000 years. *Geophys. Res. Lett.* **2003**, *30* (22), . doi: 10.1029/2003GL018169.

(36) Marino, F. Geochemical chracterization of the EPICA Dome-C ice core dust by major elements PIXE analysis and its paleo-climatic implications. PhD thesis, University of Siena, Siena, 2006.

(37) Gabrielli, P.; Planchon, F.; Hong, S.; Lee, K.; Hur, S. D.; Barbante, C.; Ferrari, C.; Petit, J.-R.; Lipenkov, V. Y.; Cescon, P.; Boutron, C. Trace elements in Vostok Antarctic ice during the last four climatic cycles. *Earth Planet. Sci. Lett.* **2005**, *234* (1−2), 249–259.

(38) Moore, J. K.; Doney, S. C.; Lindsay, K. Upper ocean ecosystem dynamics and iron cycling in a global three-dimensional model. *Global Biogeochem. Cycles* **2004**, 18. (GB4028), doi:10.1029/2004GB002220.

(39) Fung, I. Y.; Meyn, S. K.; Tegen, I.; Doney, S. C.; John, J. G.; Bishop, K. B. Iron supply and demand in the upper ocean. *Global Biogeochem. Cycles* **2000**, *14* (1), 281–295.

(40) Cassar, N.; Bender, M. L.; Barnett, B. A.; Fan, S.; Moxim, W. J.; Il, H. L.; Tilbrook, B. The Southern Ocean Biological Response to Aeolian Iron Deposition. *Science* **2007**, *317*, 1067–1070; DOI: 10.1126/science.1144602.

(41) Hinkley, T.; Pertsiger, F.; Zavjalova, L. The modern atmospheric background dust load: recognition in Central Asian snowpack, and compositional contraints. *Geophys. Res. Lett.* **1997**, *24* (13), 1607–1610.

(42) Wedepohl, K. H. The composition of the continental crust. *Geochim. Cosmochim. Acta* **1995**, *59* (7), 1217–1232.

(43) Wagenbach, D.; Ducroz, F.; Mulvaney, R.; Keck, L.; Minikin, A.; Legrand, M.; Hall, J. S.; Wolff, E. W. Sea-salt aerosol in coastal Antarctic regions. *J. Geophys. Res.* **1998**, *103* (D9), 10961–10974.

(44) Bowen, H. J. M. *Environmental Chemistry of the Elements*; Academic Press: London, 1979.

(45) Röthlisberger, R.; Mulvaney, R.; Wolff, E.; Hutterli, M.; Bigler, M.; Sommer, S.; Jouzel, J. Dust and sea salt variability in central East Antarctica (Dome C) over the last 45 kyrs and its implications for southern high-latitude climate. *Geophys. Res. Lett.* **2002**, *29* (20), 1963; doi:10.1029/2002GL015186.

(46) Bigler, M.; Röthlisberger, R.; Lambert, F.; Stocker, T.; Wagenbach, D. Aerosol deposited in East Antarctica over hte last glacial cycle: Detailed apportionment of continental and sea-salt contributions. *J. Geophys. Res.* **2006**, *111*; (D08205), doi:10.1029/2005JD006469.

(47) Ruth, U.; Barnola, J.-M.; Beer, J.; Bigler, M.; Blunier, T.; Castellano, E.; Fischer, H.; Fundel, F.; Huybrechts, P.; Kaufmann, P.; Kipfstuhl, S.; Lambrecht, A.; Morganti, A.; Parrenin, F.; Rybak, O.; Severi, M.; Udisti, R.; Wilhelms, F.; Wolff, E. EDML1: A chronology for the EPICA deep ice core from Dronning Maud Land, Antarctica, over the last 150,000 years. *Climate Past* **2007**, *3*, 475–484.

(48) Parrenin, F.; Barnola, J.-M.; Beer, J.; Blunier, T.; Castellano, E.; Chappellaz, J.; Dreyfus, G.; Fischer, H.; Fujita, S.; Jouzel, J.; Kawamura, K.; Lemieux, B.; Loulergue, L.; Masson-Delmotte, V.; Narcisi, B.; Petit, J.-R.; Raisbeck, G.; Raynaud, D.; Ruth, U.; Schwander, J.; Severi, M.; Spahni, R.; Steffensen, J. P.; Svensson, A.; Udisti, R.; Waelbroeck, C.; Wolff, E. The EDC3 chronology for the EPICA Dome C ice core. *Climate Past* **2007**, *3*, 485–497.

(49) Hinkley, T.; Matsumoto, A. Atmospheric regime of dust and salt through 75,000 years of Taylor Dome ice core: Refinement by measurement of mahor, minor, and trace metal suites. *J. Geophys. Res.* **2001**, *106* (D16), 18487–18493.

(50) Delmonte, B.; Petit, J.-R.; Basile-Doelsch, I.; Jagoutz, E.; Maggi, V., Late Quaternary Interglacials in East Antarctica from ice core dust records. In *The Climate of Past Interglacials*; Sirocko, F., Litt, T., Claussen, M., Eds.; Elsevier: Amsterdam, 2006.

(51) Siggaard-Andersen, M. L.; Gabrielli, P.; Steffensen, J. P.; Stromfeldt, T.; Barbante, C.; Boutron, C.; Fischer, H.; Miller, H. Soluble and insoluble lithium dust in the EPICA DomeC ice core - Implications for changes of the East Antarctic dust provenance during the recent glacial-interglacial transition. *Earth Planet. Sci. Lett.* **2007**, *258*, 32–43.